Turbulent mixing in strongly stratified shear flows

Hesam Salehipour, W. Richard Peltier and Colm-cille Caulfield

Department of Physics, University of Toronto
h.salehipour@utoronto.ca

Abstract

Motivated by the importance of irreversible mixing in geophysical and environmental flows, we seek to understand the dependence of its efficiency under strongly stratified conditions through a seris of direct numerical simulation of Holmboe wave instability under various initial conditions. Our numerical findings demonstrate that while mixing is enhanced when the density layer is much sharper than the shear layer, it is weakened if the background density jump across the interface increases while the background shear remains fixed. Furthermore, our results suggest that mixing efficiency of energetically turbulent flows is likely not to ever be suppressed despite arbitrarily strong stratification at the interface of a Holmboe wave.

1 Introduction

Turbulent mixing of a stably stratified flow has a leading role in controlling the rate of large scale meridional overturning circulation of the oceans (Wunsch and Ferrari, 2004). Although the precise nature of physical processes that are involved in the downscale cascade of energy, from global to dissipation scales, is not well understood, it is generally believed that shear instabilities occur as the final step in the transition to turbulence at the smallest scales (Riley and Lindborg, 2008). In addition, a layered or stepwise density structure (i.e. layers of well-mixed flow separated by sheets of sharp density interfaces), is commonly observed in nature (see e.g. Gregg (1987)). In order for fluid parcels to rise and penetrate (irreversibly) across these density interfaces, vigorous turbulent motions are required to overcome the strongly inhibitive influence of the stratification.

For a stably stratified density layer that is embedded within a shear layer of a similar finite depth, the classical Kelvin-Helmholtz instability (KHI) may grow. However if the density interface is sufficiently more localized than the shear layer, another class of shear instability, the Holmboe wave instability (HWI), emerges in spite of arbitrarily large values of stratification within the thin density inversion.

The turbulent mixing induced by these instabilities may be characterized by an efficiency, E, that quantifies the proportion of the total rate of energy dissipation which is expended on useful irreversible mixing (M). Formally E may be defined as:

$$E = \frac{M}{M + \epsilon}, \tag{1}$$

in which ϵ denotes total dissipation rate.

In the presence of strong stratification, the persistent survival of three-dimensional turbulence and thus irreversible mixing remains questionable. The relative strength of density stratification to the velocity shear may be quantified by Ri_g which is defined as,

$$Ri_g = \frac{g\Delta\rho/(\rho_0\ell_\rho)}{(\Delta U/\ell_u)^2}, \tag{2}$$

where $\Delta\rho$ and ΔU denote the density and velocity jumps across the interface and ℓ_ρ and ℓ_u represent the thickness of the density and shear layer interfaces respectively (to be defined in what follows). Notice that $R = \ell_u/\ell_\rho$ is $R \sim 1$ for KHI and $R \gg 1$ for HWI. Also recall that KHI is suppressed for $Ri_g > 1/4$ while HWI conceivably grows at arbitrarily large values of Ri.

As Ri_g increases to values larger than the Miles-Howard critical value of 1/4, it is unclear whether mixing (I) remains at its maximum efficiency, (II) asymptotes to an efficiency less than its maximum or (III) becomes completely suppressed. These three possible scenarios are illustrated in figure 1. While previous laboratory studies support (III) (Linden, 1979), recent studies seem to suggest that (II) is most likely (Strang and Fernando, 2001; Oglethorpe et al., 2013). Both cases (I) and (II) would imply the absence of a critical Richardson number as suggested by Galperin et al. (2007). Nevertheless, none of these studies discuss the vigor of turbulence as e.g. characterized by the buoyancy Reynolds number,Re_b, which represents the strength of total dissipation (ϵ) relative to the combined suppressing effects of stratification and molecular viscosity (ν), i.e.

$$Re_b = \frac{\epsilon}{\nu N^2}. \tag{3}$$

As a result, the true behavior of E with Ri_g for geophysically relevant energetic turbulence (i.e. $Re_b > 20$ (Smyth et al., 2001)) has hitherto remained enigmatic.

For example, in the context of the aforementioned shear instabilities, it is not known whether the growth of the two-dimensional Holmboe instability, which is guaranteed in spite of an arbitrarily large Ri_g, would lead to a fully three-dimensional turbulent flow. In fact, previous direct numerical simulation (DNS) of this instability at relatively low Reynolds numbers (Smyth et al., 2007) suggest that the saturated Holmboe waves may never become turbulent (i.e. $Re_b \ll 20$) which supports the notion of a complete suppression of irreversible mixing as suggested by case (III). Nonetheless, it has most recently been demonstrated in Salehipour et al. (2016a) that sufficient increase in the Reynolds number renders the induced flow truly turbulent by promoting the growth rate of the

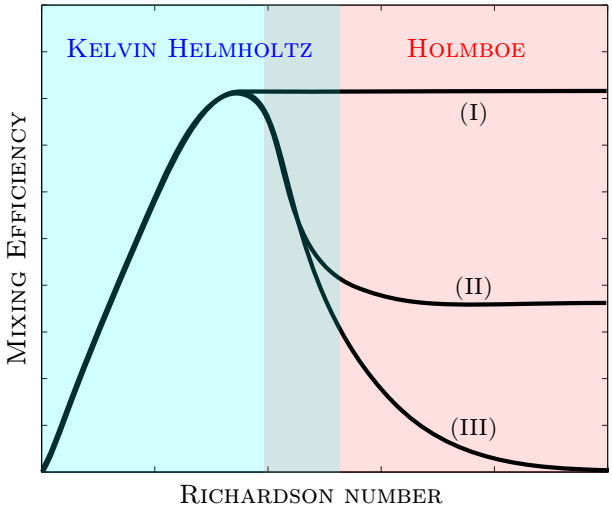

Figure 1: Schematic illustration of three hypothetical behaviors for mixing efficiency as a function of the bulk Richardson number (Ri). The shaded areas represent schematically the region of the Ri space where Kelvin-Helmholtz instability (KHI) or Holmboe wave instability (HWI) may mediate the transition to turbulence.

Table 1: Details of the three-dimensional direct numerical simulations in which the total grid points are approximately $p^3 N_x N_y N_z$ where $p = 10$ is the order of Lagrange polynomial interpolants and N_x, N_y and N_z denote the number of spectral elements within the horizontal (L_x), spanwise (L_y) and vertical (L_z) extents of the computational domain. N_z^c represents the number of elements within a central region of the domain with height $L_z^c = 10$. Outside of L_z^c, the adjacent elements of the grid are gradually stretched by a factor of 1.25%. In all these simulations, the initial Reynolds number $Re(0) = U_0 d/\nu = 6000$ and $Pr = \kappa/\nu = 8$, $L_x = \lambda$, $L_y = 3$ and $L_z = 30$ (the characteristic length and velocity scales for non-dimensionalization are $d = \ell_u(0)/2$ and $U_0 = \Delta U/2$). σ is the real part of the growth rate of the primary instability with a wavelength λ. The times t_{2d} and t_{3d} are, respectively, the characteristic time of maximum amplitude of the spanwise-averaged perturbation and the characteristic time of the maximum amplitude of the inherently three-dimensional deviation from this perturbation.

Sim.	$Ri_b(0)$	$R(0)$	$Ri_g(0)$	σ_r	λ	t_{2d}	t_{3d}	N_x	N_y	N_z	N_z^c
R3-J016	0.16	2.83	0.45	0.027	16.15	164	222	145	26	116	88
R5-J016	0.16	5	0.8	0.078	9.67	70	130	87	26	116	88
R10-J016	0.16	10	1.6	0.102	7.85	58	110	71	26	116	88
R25-J016	0.16	25	4	0.104	7.76	76	124	107	39	164	132
R5-J008	0.08	5	0.4	0.074	11.64	74	104	105	26	116	88
R10-J008	0.08	10	0.8	0.103	4.69	56	110	64	26	116	88
R5-J032	0.32	5	1.6	0.071	7.14	72	134	85	26	116	88
R10-J032	0.32	10	3.2	0.083	5.93	64	130	54	26	116	88

secondary instabilities which directly contribute to the three-dimensionalization process. Moreover, it has been shown in Salehipour et al. (2016a) that a characteristic $k^{-5/3}$ spectrum is only achieved if Re is sufficiently large.

The unknown functional variation of E with Ri_g (for $Ri_g \gg 1/4$), as depicted in figure 1, is particularly critical in a multi-parameter parameterization of E (see Salehipour et al. (2016b)). Thus, our purpose in this paper is to investigate the behaviour of HWI for increasing values of Ri_g by employing direct numerical simulation of the governing equations under the Boussinesq approximation. Since $Ri_g = RRi_b$ where Ri_b is a bulk measure of the Richardson number (sometimes also denoted by J), we will increase Ri_g separately by (i) increasing the relative thickness of the shear layer to the density layer R or (ii) by increasing Ri_b.

2 Methedology: DNS of HWI

Table 1 lists the initial conditions for the DNS cases that will be discussed in this paper. For details of the numerical methedology, boundary conditions and simulation setup, the interested reader is referred to Salehipour et al. (2015); Salehipour and Peltier (2015). The time evolving length scales associated with the shear and density layers, ℓ_u and ℓ_ρ may be defined as (Smyth and Moum, 2000),

$$\ell_u = \int_{-L_z/2}^{L_z/2} \left(1 - \overline{U}^2\right) dz, \qquad \ell_\rho = \int_{-L_z/2}^{L_z/2} \left[1 - (\overline{\rho} - 1)^2\right] dz, \tag{4}$$

where $\overline{U}$ and $\overline{\rho}$ represent non-dimensional, time-dependent velocity and and density profiles of the mean background flow which are initially fixed to be tan-hyperbolic in form.

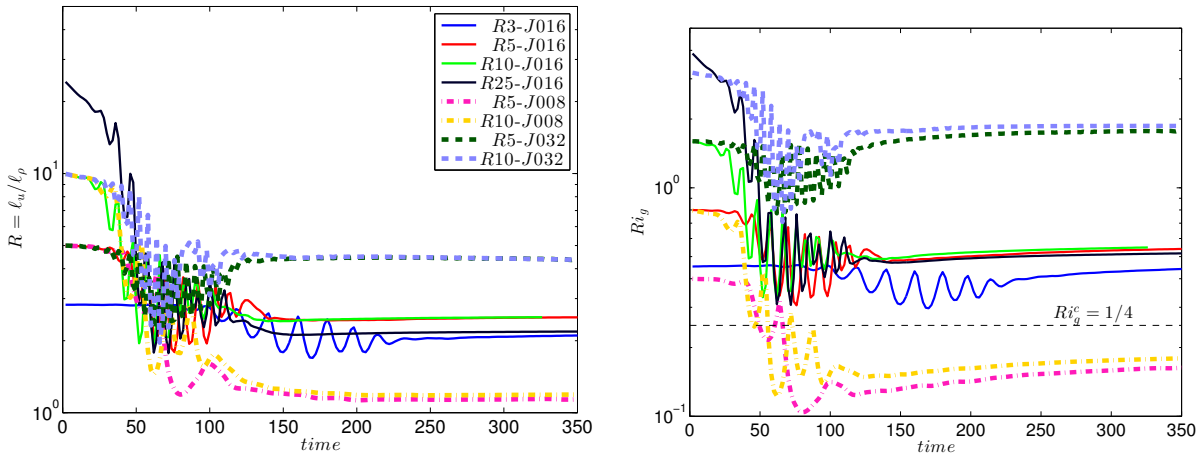

(a) (b)

Figure 2: Time evolution of (a) $R = \ell_u/\ell_\rho$ and (b) the gradient Richardson number at the interface ($z = 0$), Ri_g (see (2)) for all the DNS cases listed in table 1.

3 Results & Discussion

Figure 2 illustrates $R(t)$ and $Ri_g(t)$ for the entire life-cycle of HWI with various initial conditions as listed in Table 1. A key observation based on figure 2(a) concerns the ultimate thickness ratio, R, of these simulations. Regardless of how sharp the initial density layer is (relative to the initial shear layer), it appears that the induced turbulence adjusts non-trivially in such a way as to result in similar thickness ratios for all the cases with the same initial Ri_b (or J). For example considering case R25-J016, the ultimate thickness ratio is as large as $R \sim 2.5$, equivalent to the value obtained for all of the other cases with an initial $Ri_b = 0.16$, although its initial density interface is twenty fivefold sharper than the shear layer. As a result, while the initial conditions substantially affect the 'route to turbulence' during the transition phase, the end state is relatively robust as determined by the initial Ri_b.

A similar Ri_b-dependence is also observed if the final values of the gradient Richardson number at the interface, Ri_g, is considered (see figure 2(b)). It appears that in almost all these cases Ri_g decreases in time. This decrease is accommodated by the induced turbulent mixing which effectively tends to homogenize the flow at the interface, thus reducing Ri_g. Furthermore, as the bulk Richardson number is increased (e.g. from 0.16 to 0.32), the eventual drop in Ri_g diminishes, implying reduced mixing rates. Such a drop becomes more prominent, however, if the initial R increases (e.g. from 5 to 25 at $Ri_b = 0.16$).

We may next proceed to further investigate the impacts of varying R and Ri_b (thus changing Ri_g) on irreversible mixing. Figure 3(a) illustrates the expansion of the density layer thickness relative to its initial value, i.e. $\ell_\rho/\ell_\rho(0)$. Furthermore, the cumulative mixing, defined as $M_c(t) = \int_0^t M\, dt$, is also shown for all cases in figure 3(b). Note that M_c also represents the amount of the monotonic increase in the reference state of background potential energy in our closed system. Several interesting findings based on figure 3 follow. For a given Ri_b, as R increases the density layer expands much more significantly which is also manifest in higher cumulative mixing rates. This is consistently observed in figure 3, see e.g. simulations R5-J016 to R25-J016, all at $Ri_b = 0.16$ with varying R. In other words, the generated turbulence, after the breakdown of the primary

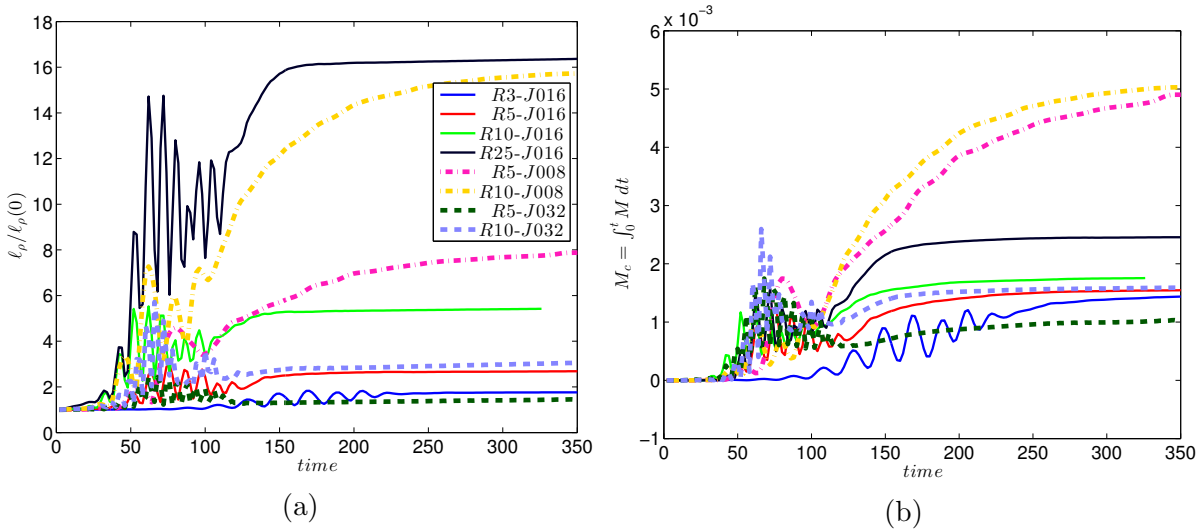

(a) (b)

Figure 3: Time dependence of (a) ℓ_ρ (see (4)) illustrating the expansion of the density layer with respect to its initial depth, and (b) Cumulative mixing, $M_c = \int_0^t M dt$ illustrating the total rise in the reference state of background potential energy. Labels for different simulations, as defined in table 1 are shown in (a).

HWI, becomes increasingly more turbulent as Ri_g increases in the presence of initially sharper density layers (i.e. higher R). On the other hand, if Ri_g increases by increasing the bulk stratification, Ri_b, it appears that the density layer expansion as well as the total amount of cumulative mixing decrease altogether. For example compare cases R5-J008, R5-J016, R5-J032 (or cases R10-J008, R10-J016, R10-J032) in figure 3. This latter finding is in accord with our observation from figure 2(a) that the thickness ratio, R, tends to decrease less as the bulk flow becomes more strongly stratified (i.e. Ri_b increases). In other words, if R remains as large as its initial value, it implies that the density layer is still sharp (small ℓ_ρ) or that it has not expanded significantly, which again translates into a reduced cumulative mixing rate. Furthermore for cases with initially high Ri_b and high R, since R remains sufficiently large at the final stage of a HWI-induced turbulence, we hypothesize that the 'old' turbulence (invoking the concept of turbulence 'age' (Smyth et al., 2001)) might 'rejuvenate' by a re-emergence of HWI.

Of course, the initial Reynolds number has been fixed to $Re = 6000$ in all the reported simulations in this paper. As Ri_b increases from 0.16 to 0.32 the vigor of turbulence declines. Nevertheless, we expect based on the discussions of Salehipour et al. (2016a), that if Re is further increased, the flow would become more energetic because not only would the growth rate of three-dimensional secondary instabilities approach their 'saturated' rate, but the inertial subrange would also tend to reveal a $-5/3$ power-law spectral behavior that is characteristic of stratified turbulent flows. In other words, we expect that at some $Re > 6000$, simulations R5-J032 and R10-J032 would lead to higher mixing rates with higher Re_b.

An extensive suit of DNS analyses associated with the growth and collapse of KHI (Salehipour and Peltier, 2015) have been employed in constructing the details of a multi-parameter parameterization for mixing efficiency as a function of a Richardson number and the buoyancy Reynolds number in Salehipour et al. (2016b). In their parameterization, Salehipour et al. (2016b) have assumed scenario (III) (see figure 1) for the Richardson number dependence of E while acknowledging the uncertainty associated with the strongly stratified region of parameter space. It is worthwhile mentioning that the Richardson

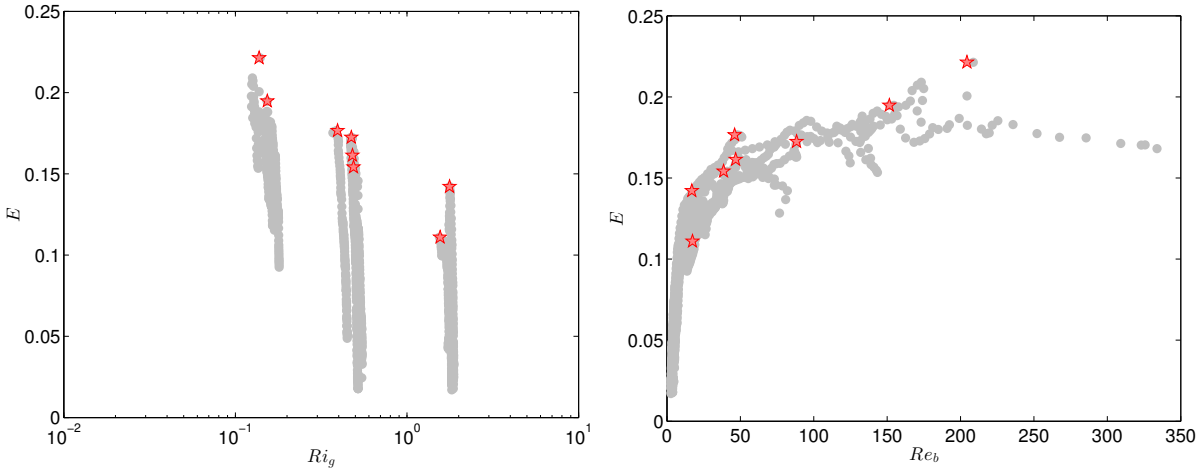

Figure 4: Variations of mixing efficiency, E (see (1)) with (a) Ri_g and (b) Re_b. Data are associated with 'mature' state of fully three-dimensional turbulence (i.e. $t \geq t_{3d}$). The peak of efficiency in each DNS case is indicated by a ★, and its corresponding Ri_g in (a) may be employed to infer the simulation labels from figure 2(b).

number may be defined in various ways and perhaps it remains to be determined which definition in the high-resolution DNS studies would be most appropriate for oceanographic applications which often involve course resolution observations. Nonetheless, in this previous work, the dependence of E on a Richardson number has been imposed in part by assuming $E^\star = f(Ri)$ where $E^\star$ represents the maximum value of E during the 'mature' stage of turbulence.

Therefore the instantaneous mixing rates of the flows studied herein due to HWI may serve to quantify the mixing efficiency, E at large values of Ri_g. Figure 4 illustrates the dependence of E on both (a) Ri_g and (b) Re_b. Notice that in this figure, we focus solely on the 'mature' stage of the flow evolution associated with fully three-dimensional turbulence. This stage is characterized here by $t \geq t_{3d}$ where t_{3d} marks the saturation point of the three-dimensional perturbation kinetic energy (see Table 1 for the reported values of t_{3d}). As discussed by Salehipour et al. (2016a), the characteristic behaviour of E during the early 'young' stage of the flow evolution (i.e. $t < t_{3d}$) highly depends on the type of primary instability (i.e. KHI or HWI) while the later more 'mature' stage is characterized by more *universal* mixing properties (Salehipour and Peltier, 2015). $E^\star$ is also shown in figure 4 by a red star and indicates the maximum mixing efficiency when the flow is most vigorously turbulent. In addition, considering that the maximum efficiency usually takes place at t_{3d} (the onset of the three-dimensional 'mature' state), the direction of time evolution (i.e. $t > t_{3d}$) is represented by the decreasing sequence of gray markers in 4(a) and leftwards in 4(b). In other words, for $t > t_{3d}$, Ri_g remains relatively constant while Re_b decreases.

The peak efficiency of the fully three-dimensional flow, $E^\star$, associated with HWI does not reach as high a level as that characteristic of KHI (i.e. 0.3-0.4 (Salehipour et al., 2016b)). Furthermore, it decreases as Ri_g increases to $Ri_g > 1/4$, thus discounting scenario (I) in figure 1, and it also appears to remain substantially above zero in contrast to scenario (III) in figure 1. In fact, it appears that $E^\star$ remains relatively fixed to the near vicinity of $E^\star \sim 0.15$ as Ri_g is increased supporting scenario (II) in figure 1. It must be emphasized that, as demonstrated by figure 4(b), the reported values of $E^\star$ are

all associated with energetic flows that can be recognized as being truly *turbulent* with $Re_b \gtrsim 20$. Previous studies (see e.g. Strang and Fernando, 2001; Oglethorpe et al., 2013) have also provided some evidence in support of scenario (II), but their results have all been obtained at $Re_b \sim \mathcal{O}(1)$ which is essentially associated with a laminar regime.

Indeed, these results should be further extended by exploring HWI with yet higher values of Ri_g. However, this may prove to be very challenging from a computational viewpoint because in order for the developed flow to be sufficiently energetic, (i.e. $Re_b > 20$), the initial Reynolds number of the DNS analyses should increase accordingly (e.g. as $Re_b \sim Re/Ri$ based on the scaling arguments of Shih et al. (2005)). Such further progress will hinge upon higher resolution DNS analyses of high-Re-high Ri_g flows.

4 Summary & Conclusions

The existence, strength and behaviour of turbulent mixing in the presence of strong density stratification has remained an open question in the literature of stratified shear flows. Motivated by this issue, we have employed direct numerical simulations to study Holmboe wave instability (HWI); a type of shear instability, which unlike its better known relative, the Kelvin-Helmholtz instability (KHI), occurs for arbitrarily large values of the gradient Richardson number at the interface (Ri_g), provided that the density layer is sufficiently sharper than the shear layer. Unlike KHI that is suppressed for the gradient Richardson numbers $Ri_g > 1/4$, under such strongly stratified conditions HWI not only emerges but also produces highly turbulent flows as discussed recently by Salehipour et al. (2016a). Although the emergence of two-dimensional HWI is expected based on linear theory alone, the transition to a fully three-dimensional turbulent flow has been achieved only by increasing the flow Reynolds number to sufficiently high values so as to lead to $Re_b > 20$ (this condition has demanded the application of large computational resources). Using a new series of DNS analyses in this paper, we have investigated the effect of changing $Ri_g = RRi_b$ (at a fixed Reynolds and molecular Prandtl number) by varying separately the thickness ratio (R), and the bulk Richardson number (Ri_b).

While the cumulative mixing and the amount of density layer expansion are both promoted for sharper initial density layers relative to the initial shear layer (i.e as R increases), they are suppressed when the bulk flow becomes more strongly stratified (i.e. higher Ri_b). The final measures of Ri_g and R do not depend on their initial values and are only determined by the initially imposed Ri_b. This suggests that the flow dynamics of HWI are adjusted non-trivially by the induced secondary instabilities and the ensuing turbulence in such a way that the final flow characteristics are determined robustly by Ri_b.

The three-dimensional turbulent flows generated by the breakdown of HWI for $Ri_g > 1/4$, provide a peak efficiency that is less than that obtained from KHI at $Ri_g \sim 1/4$. While for the latter this efficiency is approximately 0.3-0.4 (Salehipour and Peltier, 2015; Salehipour et al., 2016b), in the former case it appears to become Ri_g-independent and to asymptote to ~ 0.15 based on our results that extend to $Ri_g \sim 2$. These findings provide the first explicit evidence in support of scenario (II) (see figure 1) for strongly stratified turbulent flow with $Re_b > 20$ and suggests that the mixing induced by HWI is apparently never fully suppressed. Therefore we conjecture that scenario (II) in figure 1 is more likely to represent the characteristic behaviour of mixing efficiency so long as the flow is sufficiently energetic with $Re_b > 20$.

Further work will be required to investigate whether an 'old' state obtained from a

high-Ri_b-high-R simulation is capable of rejuvenation, as a possible mechanism for layer generation. In addition, understanding the mixing properties of HWI with high-Re-high-Ri_b initial conditions will serve to categorically establish whether scenario (II) (see figure 1) is indeed the correct characterization of mixing efficiency of strongly stratified turbulent flows.

References

Galperin, B., Sukoriansky, S., and Anderson, P. S. (2007). On the critical Richardson number in stably stratified turbulence. *Atmosp. Sci. Lett.*, 8(3):65–69.

Gregg, M. (1987). Diapycnal mixing in the thermocline: A review. *J. Geophys. Res.: Oceans*, 92(C5):5249–5286.

Linden, P. F. (1979). Mixing in stratified fluids. *Geophys. Astrophys. Fluid Dyn.*, 13:3–23.

Oglethorpe, R., Caulfield, C., and Woods, A. W. (2013). Spontaneous layering in stratified turbulent Taylor–Couette flow. *J. Fluid Mech.*, 721:R3.

Riley, J. J. and Lindborg, E. (2008). Stratified turbulence: A possible interpretation of some geophysical turbulence measurements. *J. Atmosp. Sci.*, 65(7):2416–2424.

Salehipour, H., Caulfield, C. P., and Peltier, W. R. (2016a). Turbulent mixing due to the Holmboe wave instability at high reynolds number. *J. Fluid Mech., under review.*

Salehipour, H. and Peltier, W. (2015). Diapycnal diffusivity, turbulent Prandtl number and mixing efficiency in Boussinesq stratified turbulence. *J. Fluid Mech.*, 775:464–500.

Salehipour, H., Peltier, W. R., and Mashayek, A. (2015). Turbulent diapycnal mixing in stratified shear flows: the influence of Prandtl number on mixing efficiency and transition at high Reynolds number. *J. Fluid Mech.*, 773:178–223.

Salehipour, H., Peltier, W. R., Whalen, C. B., and MacKinnon, J. A. (2016b). A new characterization of the turbulent diapycnal diffusivities of mass and momentum in the ocean. *Geophys. Res. Lett.*, 43(7):3370–3379. 2016GL068184.

Shih, L. H., Koseff, J. R., Ivey, G. N., and Ferziger, J. H. (2005). Parameterization of turbulent fluxes and scales using homogeneous sheared stably stratified turbulence simulations. *J. Fluid Mech.*, 525:193–214.

Smyth, W., Carpenter, J. R., and Lawrence, G. A. (2007). Mixing in symmetric Holmboe waves. *J. Phys. Oceanogr.*, 37:1566–1583.

Smyth, W. D., Moum, J., and Caldwell, D. (2001). The efficiency of mixing in turbulent patches: inferences from direct simulations and microstructure observations. *J. Phys. Oceanogr.*, 31:1969–1992.

Smyth, W. D. and Moum, J. N. (2000). Length scales of turbulence in stably stratified mixing layers. *Physics of Fluids*, 12:1327.

Strang, E. J. and Fernando, H. J. S. (2001). Entrainment and mixing in stratified shear flows. *J. Fluid Mech.*, 428:349–386.

Wunsch, C. and Ferrari, R. (2004). Vertical mixing, energy, and the general circulation of the oceans. *Annu. Rev. Fluid Mech.*, 36:281–314.